A modified Duvaut-Lions zero-thickness interface model for simulating the rate-dependent bond behavior of FRP-concrete joints

Antonio Caggiano[a,b,*], Enzo Martinelli[c], Diego Said Schicchi[d], Guillermo Etse[b]

[a] *Institut für Werkstoffe im Bauwesen, Technische Universität Darmstadt, Germany.*

[b] *INTECIN, Facultad de Ingeniería, Universidad de Buenos Aires and CONICET, Argentina.*

[c] *Department of Civil Engineering, University of Salerno, Fisciano, SA, Italy.*

[d] *Leibniz Institut für Werkstofforientierte Technologien (IWT), Badgasteiner Str. 3, 28359 Bremen, Germany.*

** Corresponding author, Tel.: +49-6151-16-22210; e-mail: caggiano@wib.tu-darmstadt.de (A. Caggiano), e.martinelli@unisa.it (E. Martinelli), schicchi@iwt-bremen.de (D. Said Schicchi) getse@herrera.unt.edu.er (G. Etse)*

Abstract

This paper proposes a model aimed at simulating the strain-rate effect in Fiber Reinforced Polymer (FRP) strips glued to concrete. More specifically, the loading rate-dependent bond mechanisms are evaluated by extending a classical overstress viscoplastic approach, available in the literature, generally referred to as Duvaut-Lions' approach. The model is formulated within the general theoretical framework of fracture mechanics under the assumption that debonding occurs as a pure mode II cracking process. Zero-thickness interface elements were employed for implementing the aforementioned FRP-to-concrete joint model. From the conceptual viewpoint, the model is used in an incremental analysis and the debonding phenomenon is simulated as a propagating fracture whose local residual stress is described by the decreasing branch of a bond-slip law assumed "a priori". The mechanical soundness of the proposed model is demonstrated by the very good agreement between some experimental results, taken from the scientific literature, and the corresponding numerical predictions at significantly diverse loading rates ranging from 0.07 to 70 mm/s.

Keywords: FRP; Pull-off; Visco-plasticity; Extended Duvaut-Lions; Fracture-based model.

1. Introduction

Fiber-Reinforced Polymers (FRPs) are widely employed both as internal reinforcement of new reinforced concrete (RC) constructions and external retrofitting of existing ones [1]. The externally bonding reinforcement (EBR) [2] and near-surface mounted (NSM) [3] techniques are the most employed solutions to strengthen concrete structures, mainly in bending and shear. In both cases, yet through different local mechanisms, bond between FRP strip and concrete substrate generally controls the structural response of FRP-to-concrete joints. Therefore, besides the identification of accurate bond-slip relationships, which has been duly studied in the past years [4, 5, 6], several critical aspects are currently under investigation.

The integrity of the FRP-to-concrete interface in aggressive outdoor environments is one of those aspects. Deterioration modeling, non-destructive methods for field evaluation and emerging developments in design, specifications and product approval have been reviewed and discussed in a recent paper [7]. Moreover, the performance under fire exposure of FRP-strengthened RC structural members is another issue of current relevance in the scientific literature. The mechanical behavior at high temperature of the constituent materials of FRPs and how their bond to concrete is affected when heated have been investigated [8]. Furthermore, the consequences of blast and impact actions on structures has attracted the attention of the technical and scientific communities. Experimental evidences show that FRP can be also used as an excellent material to improve the resistance of concrete structures under these actions [9, 10].

Bonding of a FRP plate to the tension face of a beam is one of the most common flexural strengthening method employed. Plenty of studies have been carried out in the last decades with the special aim to investigate and simulate the behavior of FRP-strengthened RC beams [11, 12]. Moreover, national and international guidelines have adopted some of those models leading to a wider spectrum of possible applications for FRP composites in structural engineering [13, 14]. Nevertheless, among the various aspects regarding the mechanical behavior of FRP-strengthened concrete members, simulating the bond interaction between FRP strips and concrete substrate has been recognized as a major and key issue in this field. Complex phenomena, such as failure induced by cyclic loading or fire exposure, have been recently taken into account in order to numerically simulate these events in FRP-to-concrete joints. For instance, Martinelli and Caggiano [15] formulated a model capable to reproduce the (low cyclic) fatigue behavior of FRP strips externally bonded to concrete by considering both bi-linear and linear-exponential bond-slip laws (both based on Fracture Me-

chanics concepts), yet under the assumption of a quasi-static load application process. Caggiano and Schicchi [16] worked on a thermo-mechanical model for modeling the bond responses of FRP strips glued to concrete substrates exposed to elevated temperature. Nonetheless, in spite of these efforts, no much scientific literature is available regarding strain-rate effects on the bonding response. Actually, most research has been mainly focused on the behavior under monotonic actions and quasi-static loading processes [17], even though FRP is often employed in enhancing the structural performance of concrete members subjected to cyclic loads applied at significant strain rates[18].

As far as strain-rate is of concern, relatively few experimental studies have been conducted to evaluate the dynamic response of FRP-concrete interfaces [19, 20]. Particularly, Shen et al. [21] presented an experimental investigation of the dynamic performance between Basalt-Fiber Reinforced Polymer (BFRP) sheets and concrete under different strain rates in double-lap shear tests.

It is noted that the majority of the existing models and/or numerical procedures, which are in reasonable agreement with experimental pull-off results on FRP-to-concrete joints [22, 23], mainly neglect the effect of strain rate on the bond behavior of the FRP-to-concrete interface. This paper aims at proposing a model capable to simulate the response of FRP-to-concrete joints subjected to monotonic loads, but taking into account the strain rate effects. In the Authors' opinion, the most attractive feature of the proposed formulation is that the main physical quantities of relevance in Fracture Mechanics, such as the inelastic work spent in the fracture process, can be expressed in closed-form, while strain rate effects are taken into account through a modification of the well-known Duvaut-Lions overstress viscoplastic approach [24, 25, 26, 27].

After this general introduction about the state-of-the-art and main motivation of this research, the paper is organized as follows. Section 2 outlines the fundamental theoretical assumptions of the proposed model. Section 3 discusses the inviscid formulation while Section 4 presents its viscoplastic extension. Section 5 proposes the model validation and reports some comparisons between a series of experimental results, available in the scientific literature and here assumed as benchmark, and the corresponding numerical simulations. Lastly, Section 6 remarks the main findings of this study and introduces the future development of this research.

2. Bond behavior of FRP-to-concrete joint: fundamental assumptions

The model is based on the following fundamental assumptions:

- FRP strips are modeled as an elastic material. One-dimensional two-nodes isoparametric trusses are employed;
- debonding process develops at the FRP-to-concrete interface in pure "mode II": hence, zero-thickness interface elements are used for this purpose;
- softening is modeled by means of the post-elastic exponential branch of the bond-slip law, for which a closed-form exponential expression is assumed;
- stiffness degradation in the unloading-reloading stages depends on the current value of the "fracture work" spent at each (Gauss-) point of the FRP-to-concrete interface;
- displacements are supposed to be "small";
- Concrete substrate is assumed to be a rigid block supporting the FRP plate: therefore, the concrete-adhesive interface is supposed to be fully-fixed in the numerical model.

The aforementioned assumptions lead to defining the mechanical governing equations in terms of a rate-independent model, presented in Section 3. Afterward, in Section 4 the model is extended with the aim to consider the strain rate effects. Particularly, the adhesive layer between the FRP laminate and the concrete substrate is simulated through a visco-elasto-plastic constitutive relationship for interface elements. This constitutive model, which reproduces the dynamic nonlinear response of the FRP-to-concrete joints, is formulated within the general framework of fracture mechanics combined with viscoplastic effects.

It is worth highlighting that all mechanical nonlinearities, adopted in the aforementioned formulations and assumptions, are lumped at the interface between the FRP laminate and the concrete substrate. Particularly, the numerical implementation was performed by programming the proposed zero-thickness interface model into a *user-defined* interface constitutive law (UINTER) of Abaqus®, developed ad-hoc by the Authors.

Figure 1 shows the FRP strip glued to a concrete block and a schematic representation of the interfacial shear stresses.

3. Inviscid formulation

Considering a uniform width (b_f) and thickness (t_f) along with a unique bond-slip relationship throughout the whole adhesive interface, the following equilibrium condition can be stated:

$$\frac{d\sigma_p[x]}{dx} = -\frac{\tau[x]}{t_p} \tag{1}$$

being $\tau[x]$ the interface bond stress and $\sigma_p[x]$ the axial stress in the FRP cross section.

The interface bond-slip law, proposed by the authors and employed in a previous work [15], is described by means of the following linear-(negative-)exponential relation (Figure 2):

$$\begin{cases} \tau[x] = -k_E\, s[x] & \text{if } s[x] \le s_e \\ \tau[x] = -\tau_0\, e^{-\beta(s[x]-s_e)} & \text{if } s[x] > s_e \end{cases} \tag{2}$$

where k_E is the (positive scalar) tangential bond stiffness in pre-peak response, $s[x]$ the shear slip at the considered x abscissa, $s_e = \tau_0/k_E$ represents the elastic slip value, τ_0 is the shear strength, and β is a parameter for describing the post-peak shape of the $\tau - s$ rule.

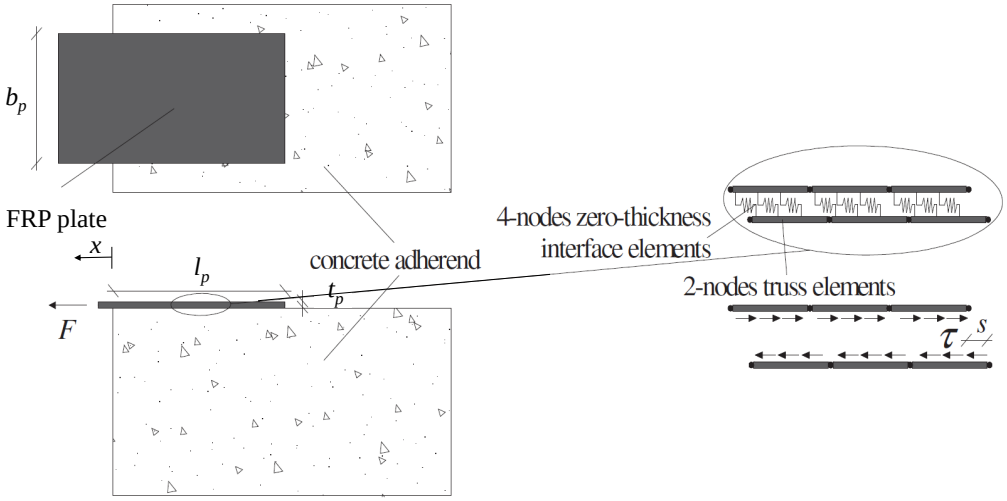

Figure 1: Single-lap shear test of a FRP-to-concrete bonded joint.

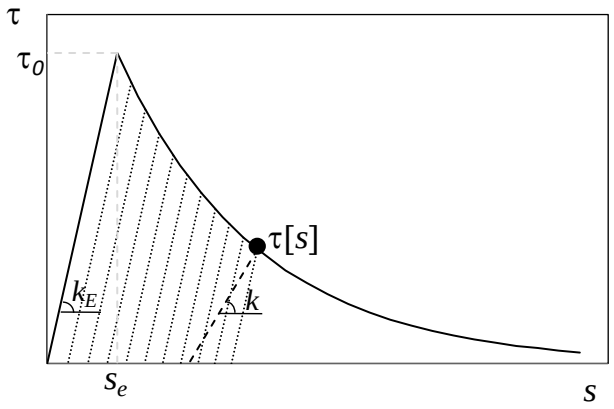

Figure 2: Bond-slip law highlighting the fracture work spent.

As already mentioned, the FRP strip follows a linear elastic behavior in terms of axial stress versus strain, i.e.:

$$\sigma_p[x] = E_p \varepsilon_p \tag{3}$$

where E_p is the Young's modulus of the composite.

The strain field can be calculated by means of the compatibility condition according to:

$$\varepsilon_p = \frac{ds[x]}{dx}. \tag{4}$$

By introducing Eq. (4) into (3) and, thereafter, into the equilibrium condition given by Eq. (1), the following well-known differential equation is obtained:

$$\frac{d^2 s[x]}{dx^2} + \frac{\tau[x]}{E_p\, t_p} = 0. \tag{5}$$

The stiffness under unloading/reloading conditions is accounted by considering, for each point of the adhesive interface, the ratio between the current inelastic spent work w_{sl} and the corresponding fracture energy (in pure "mode II"), G_f^{II}. The accumulated cracking spent work, namely w_{sl}, developed during the sliding fracture process, controls the damage evolution. This variable mainly deals with the "inelastic part" of the enclosed area of the $\tau - s$ curve (see Figure 2).

Hence, the inelastic work spent in the fracture process can be expressed in closed-form as follows:

$$\begin{aligned} w_{sl} &= \int_0^s |\tau[x]|\, dx - \frac{\tau[x]}{2\, k_E} \\ &= \frac{k_E\, s_e^2}{2} \left\{ 1 - e^{-2\beta(s[x]-s_e)} - \frac{2\left(e^{-\beta(s[x]-s_e)} - 1\right)}{\beta s_e} \right\} \end{aligned} \tag{6}$$

where $w_{sl} = 0$ for $s[x] = s_e$.

The total inelastic work spendable, which actually represent the fracture energy G_f^{II}, depends on the key parameters involved in Eq. (6). Its calculation follows the below relationship:

$$\begin{aligned} G_f^{II} &= \int_0^\infty |\tau[s]|\, ds \\ &= \frac{k_E\, s_e^2}{2} \left(1 + \frac{2}{\beta s_e} \right). \end{aligned} \tag{7}$$

The damage parameter d can be thus defined in each point of the adhesive interface as

$$d = \left(\frac{w_{sl}}{G_f^{II}} \right)^{\alpha_d} \tag{8}$$

where α_d controls the shape of the damage curve.

Finally, the loading/unloading stiffness k is related to the elastic one through the following relationship:

$$k = k_E\, (1 - d)\,. \tag{9}$$

4. Viscoplastic extension

In order to capture strain-rate phenomena occurring at the bond between FRP sheets and concrete substrates, a modified

version of the classical Duvaut-Lions visco-plastic model [28] is considered to extend the previous formulation.

4.1. Duvaut-Lions viscoplastic approach

In the Duvaut-Lions rate-dependent approach, also known as viscoplastic correction, the instantaneous response is directly related to the inviscid material behavior as it is based on the assumption that the return of the stress state to the yield surface (fulfilling the condition $f = 0$, being f the yielding condition of the model) does not take place immediately but with some delay, according to the flow rule (applied to the interface):

$$\dot{s}_{vp} = \frac{{k_E}^{-1}}{\eta}\left(\tau^e - \tau_p\right) = \dot{s}_0^{vp} - \dot{s}_\infty^{vp} \tag{10}$$

where $\dot{s}_{vp}$ is the general viscoplastic slip rate, η is the material viscosity, τ^e the elastic interfacial stress and τ_p the stress state obtained from the solution of the inviscid problem. Thus, under constant stress, the inelastic strain (slip) rate is constant and proportional to the overstress, namely $\tau^e - \tau_p$. The time-dependent kinematic solution is found interpolating between the instantaneous solution (elastic increment, $\dot{s}_0^{vp}$) and the inviscid one (elastoplastic increment, $\dot{s}_\infty^{vp}$).

After introducing the linearized flow rule of Duvaut-Lions in the Prandtl-Reuss decomposition law of the total slip rate, the following form can be obtained for the increment of the stress:

$$\Delta\tau_{vp} = \left(1 - \frac{\Delta t}{\eta}\right)\Delta\tau_{\mathtt{trial}} + \frac{\Delta t}{\eta}\Delta\tau_{ep} \tag{11}$$

where $\Delta\tau_{vp}$ is the viscoplastic stress increment, $\Delta\tau_{\mathtt{trial}}$ is the trial elastic stress increment, and $\Delta\sigma_{ep}$ the inviscid stress increment.

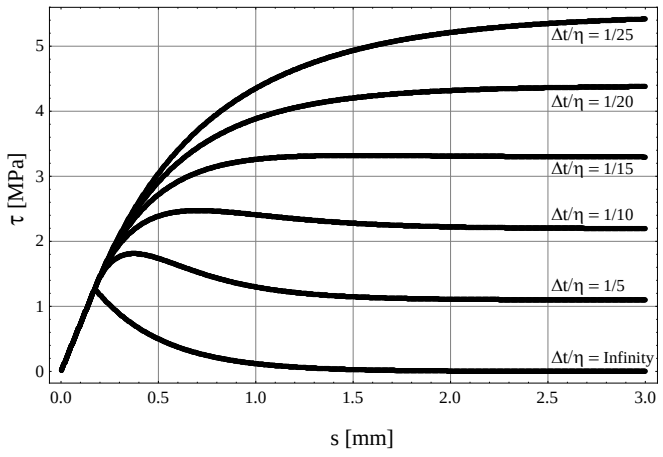

Figure 3: Bond-slip law highlighting the strain-rate effect modeled with the Duvaut-Lions procedure. Adopted parameters are: interfacial shear stiffness $k_E = 7.32\,MPa/mm$, peak interfacial shear stress $\tau_0 = 1.270\,MPa$, mode II fracture energy $G_f^{II} = 0.554\,N/mm$ and $\alpha_d = 1.0$.

4.2. Modified Duvaut-Lions viscoplastic approach

For the purpose of the rate-dependent interface model formulation in this work, a modified version of the Duvaut-Lions viscoplastic formulation is proposed. More specifically, at each contact point of the adhesive interface, the modified Duvaut-Lions-based viscoplastic correction is applied instead, as follows:

$$\tau_{n+1}^f = e^{-(\Delta t/\eta)^\alpha}\tau_n + \left(1 - e^{-(\Delta t/\eta)^\alpha}\right)\tau_{n+1} + \frac{1 - e^{-(\Delta t/\eta)^\alpha}}{(\Delta t/\eta)^\alpha}\Delta\tau \tag{12}$$

where τ_{n+1}^f represents the viscoplastic total bond-slip stress at time-step "n+1", τ_n and τ_{n+1} are the inviscid total bond-slip stress at time-step "n" and "n+1", respectively, and $\Delta\tau$ is the trial elastic bond-slip stress increment between the time-steps "n" and "n+1". In addition, Δt is the considered step time increment, while η [sec.] and α (>0 and dimensionless) are viscoplastic parameters.

Depending on η values, the following two extreme cases can occur:

$$\begin{cases} \eta \to 0 & \tau_{n+1}^f = \tau_{n+1} \quad \text{Inviscid response} \\ \eta \to \infty & \tau_{n+1}^f = \tau_n + \Delta\tau \quad \text{Elastic response} \end{cases} \tag{13}$$

Figure 3 shows possible visco-plastic responses by considering decreasing values of the ratio $\Delta t/\eta$. The case $\Delta t/\eta$ = "Infinity" mainly represents the inviscid response while rising values of η allows to obtain an increment of the apparent strength as result of the strain-rate effect.

It is worth to mention that the simulation of visco-plastic responses based on overstress-based models, such as those based upon the Duvaut-Lions approach, consist of "interpolating" the purely inviscid inelastic behavior and the fully elastic response. Therefore, residual stresses are always present for high values of interface slips, which do not allow to simulate the complete debonding of the glued plate without generating residual pull-off forces. However, this is a well-known (and often accepted) limitation of the Duvaut-Lions approach, alternative approached may be developed in the future as further evolutions of the present research [29].

5. Loading rate effects under monotonic loads

As it was briefly commented in the introductory section, the study of Shen et al. [21] is here considered as experimental benchmark for validation purposes of the proposed formulation. The simulation of the strain rate effect is performed by considering a series of test results on modified double-lap shear tests, which followed the test recommendation by JSCE [30].

The experimental data corresponds to the bond behavior of BFRP sheets glued to concrete substrates. Even though these experimental tests are performed on double-lap shear schemes, the present simulations are based on a single-lap shear test in view of reducing computational costs of the analysis. Therefore, the experimental measurements, both in terms of forces

and slips, have been halved to be compared with the corresponding numerical simulations: this is based on assuming perfect symmetry for the double-lap shear tests, which is reasonable for the pre-peak response and in case of simultaneous debonding, thus maintaining the perfect symmetry in post-peak regime [31].

In the experimental campaign, each specimen consisted of a 510-mm-long concrete block with a 100 x 100 mm^2 cross-section. Basalt-FRP (BFRP) sheets with $b_p = 50\,mm$ width and $t_p = 0.121\,mm$ thickness were bonded with epoxy resin on two opposite sides of the concrete blocks along their axial direction. The bonded length for all specimens was $200\,mm$. BFRP sheets had a mean relative axial stiffness $E_p\,t_p = 12.7\,kN/mm$.

The experimental test set-up allowed to impose a dynamic load with a displacement rates of 0.07, 0.7, 7, and 70 mm/s to reach the complete failure. The numerical analyses were run in displacement control, by assuming an invariant displacement increment. Conversely, different time steps were assumed with the aim to obtain the aforementioned displacement rates.

Specimens were labeled as L200-D0, L200-D1, L200-D2, and L200-D3, for each one of the aforementioned loading-rate. This nomenclature was given in the original publication and here maintained. Three experimental specimens were available for each loading history case whose curves can be found next in Figures 4(a-d).

The consequent numerical examples refer to these main geometric details, material properties and strain rate protocols described by the experimental evidences [21]. A constant value for the Young's modulus of BFRP, $E_p = 105\,GPa$, is assumed according to [21]. Moreover, the values of the relevant material parameters identified for the numerical simulation and aimed at reproducing the experimental curves, are:

- the shear stiffness $k_E = 7.32\,MPa/mm$,
- the bond strength $\tau_0 = 1.270\,MPa$,
- the mode II fracture energy $G_f^{II} = 0.554\,N/mm$, and
- the viscosity parameter $\eta = 1.75\text{x}10^{-2}\,s$ and
- shape parameters $\alpha = 0.25$.

The first three parameters (k_E, τ_0 and G_f^{II}) mainly control the inviscid bond-slip response of the numerical model, contrarily η and α account for the Duvaut-Lions description. A sensitivity analysis has been previously performed in order to choose the minimum numbers of FE to be employed with the aim of reducing discretization errors. After that, 80 interface elements were finally adopted in the FE results which are shown in this section.

Figure 4 compares the experimental results against the numerical predictions, in terms of applied force versus slip. Particularly, Figures 4(a-d) respond to the different applied slip rates, i.e.: 0.07, 0.7, 7 and 70 mm/s, respectively. Numerical results were obtained by assuming the proposed viscoplastic fracture-based discontinuous model. The agreement between the experimental data and numerical results is highly satisfactory as demonstrated by the mentioned comparisons. It is worth to mention that the same sets of calibrated interface parameters were employed in all analysis which further highlight the capability of the proposal to capture the loading rate effects in FRP-to-concrete bonds.

The strain rate effects on the ultimate load of the FRP-to-concrete interface is highlighted in Figure 5, where the four aforementioned numerical responses are plotted, all together, and compared. The ultimate load capacity of the BFRP-concrete interface, when increasing strain rate of loading are considered, is quite evident for the "converted" double-lap simulations. The dynamic ultimate loads obtained from the numerical simulations are 11.9, 12.3, 12.9 and 14.1 kN for specimens L200-D0, L200-D1, L200-D2, and L200-D3, respectively. Thus, it means that when the loading rates raises from 0.07 mm/s to 0.7, 7.0 and 70.0 mm/s, the dynamic ultimate load increases at the rates of 3.4, 8.4, and 18.5 %, respectively. These values are also in a very good agreement with the experimental observations proposed by Shen et al.[21].

A further representation of the loading rate effect can be drawn out by observing the evolution of both the axial strain and interface shear stress fields. The comparison in terms of the numerically determined axial strain distributions of the BFRP and the corresponding interfacial shear stresses in the bond length are shown in Figures 6 and 7, respectively. Each one of the 4 subfigures exhibits the results of a single loading rate, where a series of 5 curves present the results for different load levels expressed in terms of pull-off displacement frontiers. Particularly, it is observed in Figure 6 how the debonding evolution generates the transition from a convex shape (s=0.25 mm) of the deformed configuration to a concave one (s=1.5 mm), followed by the post-peak response (s=2.0 mm) up to the final failure. Accompanying this evolution, the maximum interface stress moves from the very left, at the beginning of the test (s=0 mm), up to its residual value in case of final failure (see Figure 7).

Moreover, Figure 8 compares the loading rate effects on both the axial strains developed throughout the BFRP strip and interfacial shear stress determined at different levels of the maximum imposed slip (namely, 0.25, 1.0 and 2.0 mm) with the four displacement-rates considered in this study. Figure 8a) and b) refer to the case of an imposed slip of 0.25 mm: in this case, the difference between the response under different displacement-rates is almost negligible. The interface slip distribution (8a) is similar to the one obtained in quasi-static (inviscid) conditions; minor difference appear in terms of shear stresses around the loaded end of the strip, with, as expected, the higher stresses resulting from the faster displacement-rate (8b). Figure 8c) and d) represent the results obtained at an imposed slip of 1.0 mm. The overstressed deriving by the strain rate effect simulated according to the Duvaut-Lions approach are more apparent in this case, especially in the right part of the bond length that is actually in softening. Lastly, the fully concave curves represented in Figure 8e) demonstrate that all the bond length is in the post-elastic branch, as the maximum imposed slip (2.0 mm) is far greater than the elastic one. Moreover, Figure 8f) highlights the expected overstress arising for the higher applied slip rates.

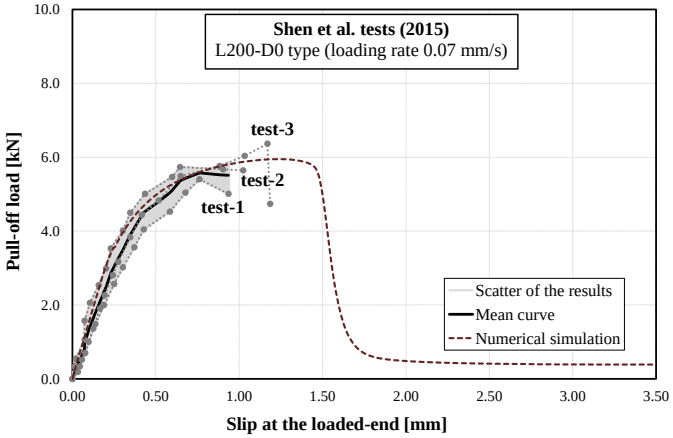

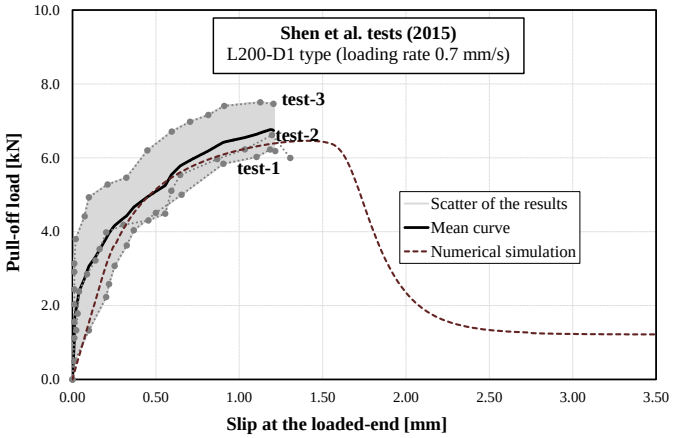

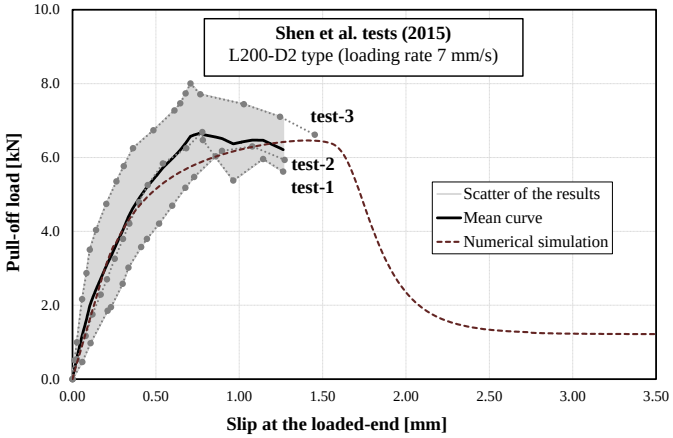

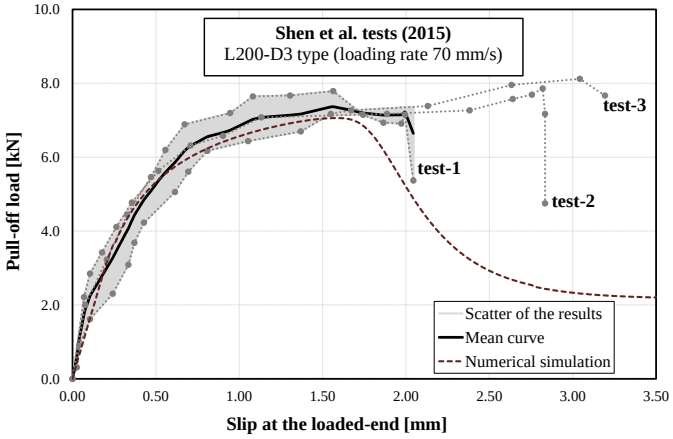

Figure 4: Load-slip curves: experimental results [21] vs. numerical analyses for (a) 0.07 mm/s, (b) 0.7 mm/s, (c) 7 mm/s and (d) 70 mm/s.

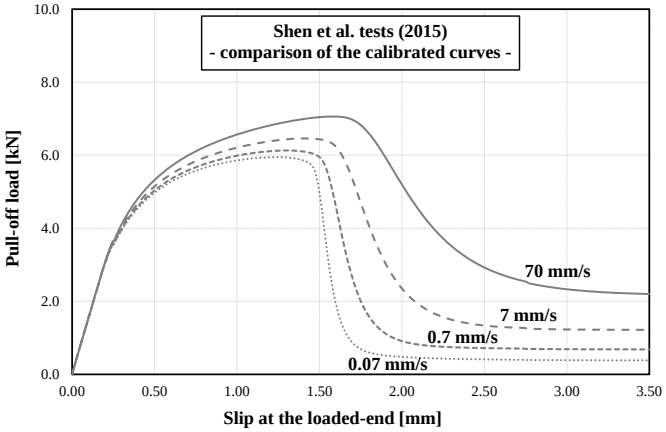

Figure 5: Comparison of the numerical responses of different strain rates.

6. Conclusions

This paper is intended as a contribution for the understanding of the mechanical behavior of FRP strips glued to concrete subjected to strain rate effects. Particularly, the following key items can be remarked:

1. the proposed model has been formulated within the general framework of Fracture Mechanics and assumed an exponential-based rule for the softening description of the bond-slip relationship;
2. a viscoplastic extension of the interface model was then proposed for taking into account the rate-dependent effects by means of a modified Duvaut-Lions overstress approach was proposed;
3. the comparison between some experimental results available in the literature and the numerical simulations performed by means of the present model highlighted its high predictive potential for different strain-rate regimes.
4. The dynamic ultimate load of the BFRP-to-concrete interface increases as the strain rate increases. Particularly, the influence of the strain rate in the dynamic ultimate load has been observed experimentally and automatically captured with this formulation.

To the Authors' best knowledge, these results have not been well highlighted yet in the international scientific literature, especially through numerical analyses. This research line will be continued in order to further validate the model with reference to cyclic tests characterized by various loading protocols combined with strain-rate regimes.

Acknowledgments

The Alexander von Humboldt-Foundation is acknowledged for funding the research position of Dr. A. Caggiano at the Institute of Construction and Building Materials at TU-Darmstadt under the research grant ITA-1185040-HFST-(2CENENRGY

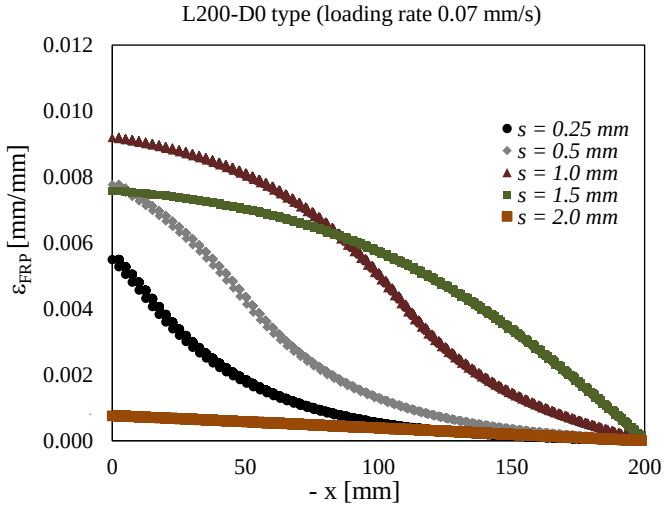
L200-D0 type (loading rate 0.07 mm/s)
0.012
0.010
0.008
0.006
0.004
0.002
0.000
εFRP [mm/mm]
0
50
100
150
200
- x [mm]
s = 0.25 mm
s = 0.5 mm
s = 1.0 mm
s = 1.5 mm
s = 2.0 mm

(a)

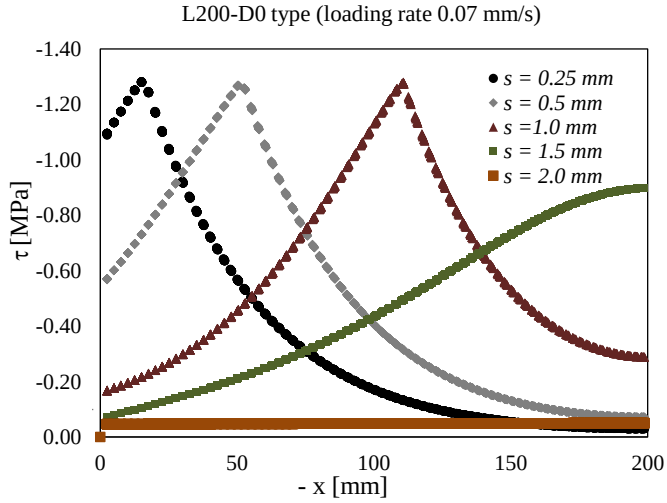
L200-D0 type (loading rate 0.07 mm/s)
-1.40
-1.20
-1.00
-0.80
-0.60
-0.40
-0.20
0.00
τ [MPa]
0
50
100
150
200
- x [mm]
s = 0.25 mm
s = 0.5 mm
s =1.0 mm
s = 1.5 mm
s = 2.0 mm

(a)

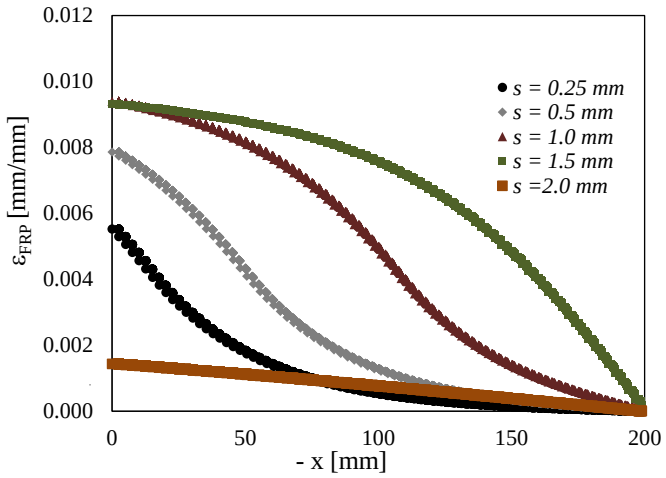
L200-D1 type (loading rate 0.7 mm/s)
0.012
0.010
0.008
0.006
0.004
0.002
0.000
εFRP [mm/mm]
0
50
100
150
200
- x [mm]
s = 0.25 mm
s = 0.5 mm
s = 1.0 mm
s = 1.5 mm
s =2.0 mm

(b)

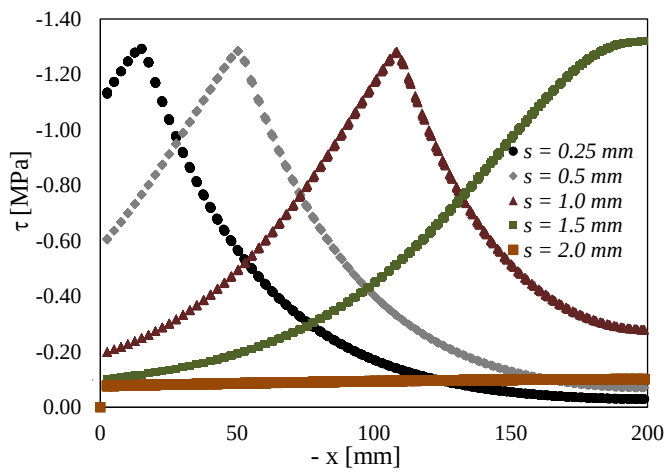
L200-D1 type (loading rate 0.7 mm/s)
-1.40
-1.20
-1.00
-0.80
-0.60
-0.40
-0.20
0.00
τ [MPa]
0
50
100
150
200
- x [mm]
s = 0.25 mm
s = 0.5 mm
s = 1.0 mm
s = 1.5 mm
s = 2.0 mm

(b)

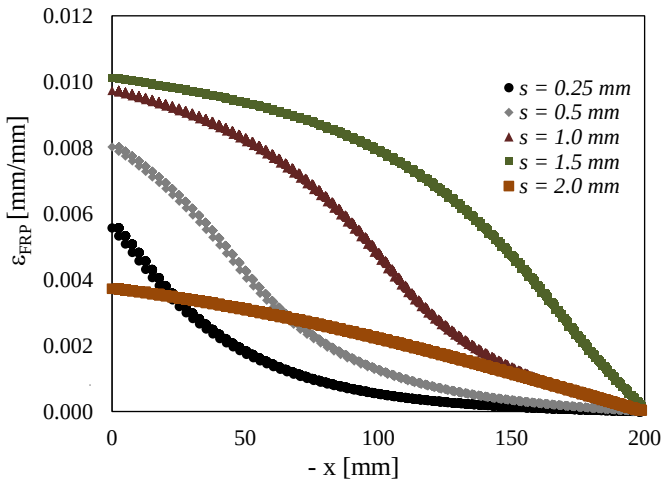
L200-D2 type (loading rate 7 mm/s)
0.012
0.010
0.008
0.006
0.004
0.002
0.000
εFRP [mm/mm]
0
50
100
150
200
- x [mm]
s = 0.25 mm
s = 0.5 mm
s = 1.0 mm
s = 1.5 mm
s = 2.0 mm

(c)

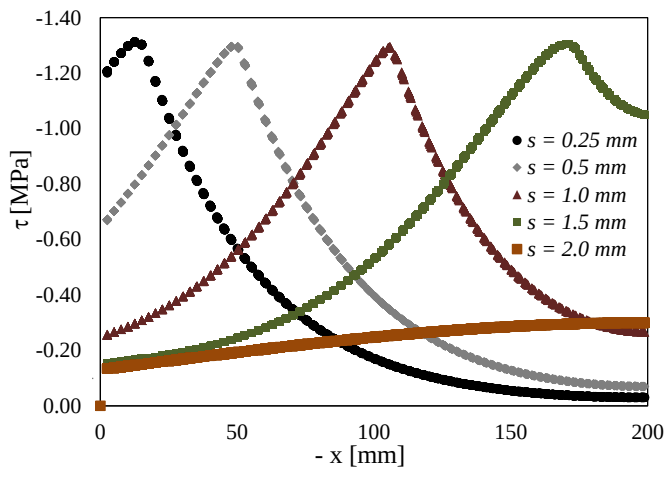
L200-D2 type (loading rate 7 mm/s)
-1.40
-1.20
-1.00
-0.80
-0.60
-0.40
-0.20
0.00
τ [MPa]
0
50
100
150
200
- x [mm]
s = 0.25 mm
s = 0.5 mm
s = 1.0 mm
s = 1.5 mm
s = 2.0 mm

(c)

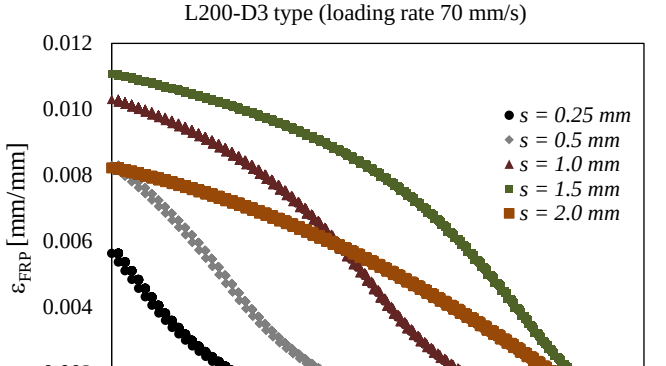
L200-D3 type (loading rate 70 mm/s)
0.012
0.010
0.008
0.006
0.004
εFRP [mm/mm]
s = 0.25 mm
s = 0.5 mm
s = 1.0 mm
s = 1.5 mm
s = 2.0 mm

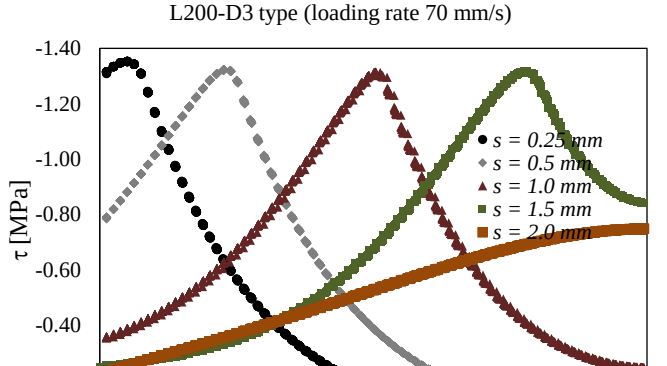
L200-D3 type (loading rate 70 mm/s)
-1.40
-1.20
-1.00
-0.80
-0.60
-0.40
τ [MPa]
s = 0.25 mm
s = 0.5 mm
s = 1.0 mm
s = 1.5 mm
s = 2.0 mm

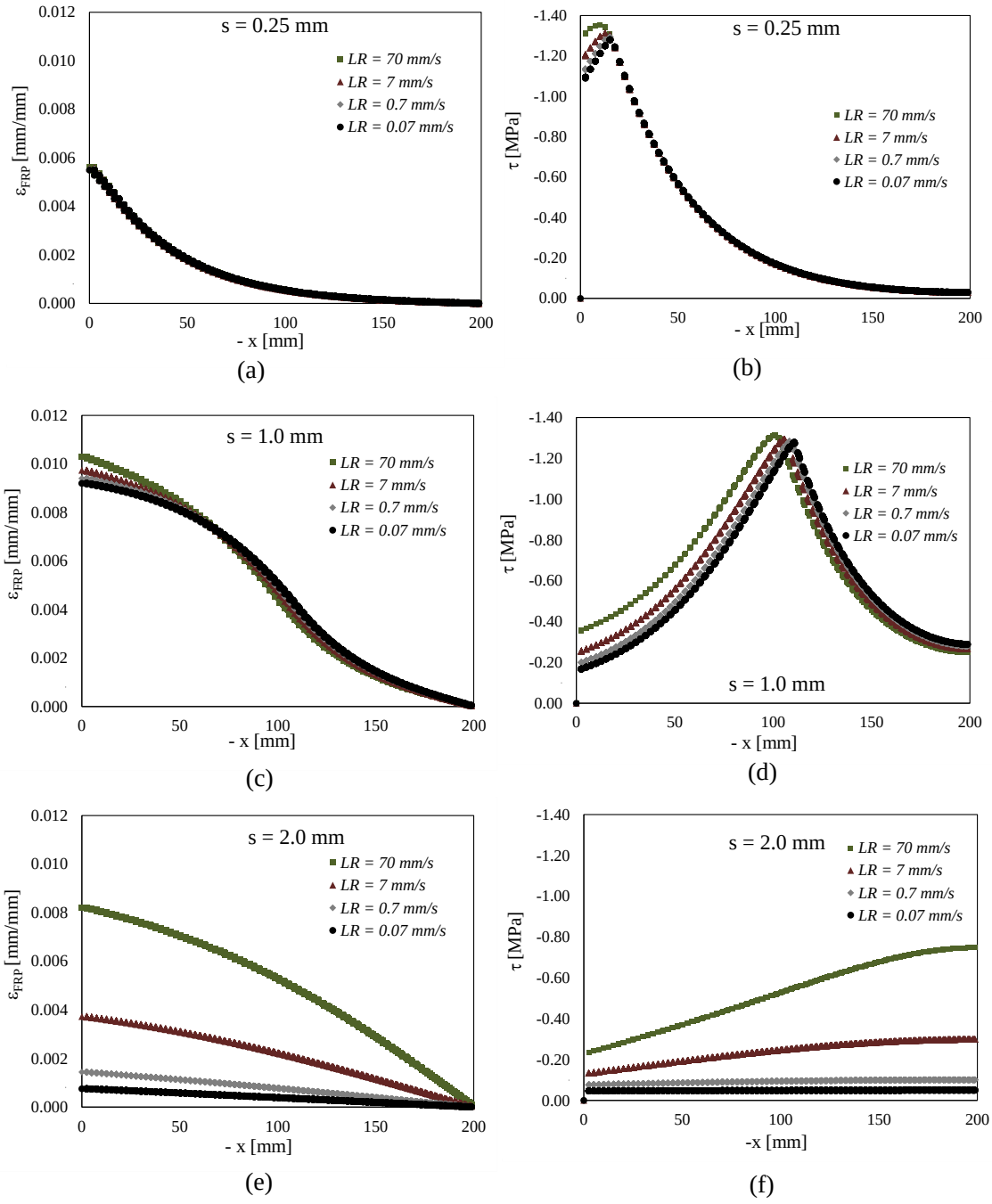

Figure 8: Comparison of the axial strain distributions (a-c-e) and interfacial shear stresses (b-d-f) along the bonding length for different strain rates for different imposed slips.

project). Moreover, the support to networking activities provided by the SUPERCONCRETE Project (H2020-MSCA-RISE-2014 n 645704; http://www.superconcreteh2020.unisa.it/) funded by the European Union is also gratefully acknowledged.

7. Reference

[1] Hollaway, L.. A review of the present and future utilisation of FRP composites in the civil infrastructure with reference to their important in-service properties. Construction and Building Materials 2010;24(12):2419–2445.

[2] Dalalbashi, A., Ghiassi, B., Oliveira, D.V., Freitas, A.. Effect of test setup on the fiber-to-mortar pull-out response in trm composites: Experimental and analytical modeling. Composites Part B: Engineering 2018;143:250–268.

[3] Coelho, M.R., Sena-Cruz, J.M., Neves, L.A.. A review on the bond behavior of FRP NSM systems in concrete. Construction and Building Materials 2015;93:1157–1169.

[4] Hadigheh, S., Gravina, R.. Generalization of the interface law for different frp processing techniques in frp-to-concrete bonded interfaces. Composites Part B: Engineering 2016;91:399–407.

[5] Chen, C., Cheng, L.. Theoretical solution to fatigue bond stress distribution of nsm frp reinforcement in concrete. Composites Part B: Engineer-

ing 2016;99:453–464.
[6] Coelho, M., Neves, L., Sena-Cruz, J.. Designing nsm frp systems in concrete using partial safety factors. Composites Part B: Engineering 2018;139:12–23.
[7] Sen, R.. Developments in the durability of FRP-concrete bond. Construction and Building materials 2015;78:112–125.
[8] Firmo, J.P., Correia, J.R., Bisby, L.A.. Fire behaviour of FRP-strengthened reinforced concrete structural elements: a state-of-the-art review. Composites Part B: Engineering 2015;80:198–216.
[9] Buchan, P., Chen, J.. Blast resistance of FRP composites and polymer strengthened concrete and masonry structures: A state-of-the-art review. Composites Part B: Engineering 2007;38(5-6):509–522.
[10] Pham, T.M., Hao, H.. Review of concrete structures strengthened with FRP against impact loading. In: Structures; vol. 7. Elsevier; 2016, p. 59–70.
[11] Smith, S.T., Teng, J.. FRP-strengthened RC beams. I: review of debonding strength models. Engineering structures 2002;24(4):385–395.
[12] Teng, J., Chen, J.F., Smith, S.T., Lam, L.. FRP: strengthened RC structures. Frontiers in Physics 2002;:266.
[13] CNR-DT200 R1, Guide for the design and construction of externally bonded FRP systems for strengthening existing structures - Materials, RC and PC structures, masonry structures (first revision). Consiglio Nazionale delle Ricerche, Italia 2013;.
[14] ACI 440.-2R-17, Guide for the design and construction of externally bonded FRP systems for strengthening concrete structures. American Concrete Institute 2017;.
[15] Martinelli, E., Caggiano, A.. A unified theoretical model for the monotonic and cyclic response of FRP strips glued to concrete. Polymers 2014;6(2):370–381.
[16] Caggiano, A., Schicchi, D.S.. A thermo-mechanical interface model for simulating the bond behaviour of FRP strips glued to concrete substrates exposed to elevated temperature. Engineering Structures 2015;83:243–251.
[17] Kang, T.H.K., Howell, J., Kim, S., Lee, D.J.. A state-of-the-art review on debonding failures of FRP laminates externally adhered to concrete. International Journal of Concrete Structures and Materials 2012;6(2):123–134.
[18] Teng, X., Zhang, Y.. Structural behavior FRP-strengthened steel-reinforced concrete slabs under moving-wheel cyclic loads. Australian Journal of Structural Engineering 2017;18(2):86–94.
[19] Shen, D., Shi, H., Ji, Y., Yin, F.. Strain rate effect on effective bond length of basalt FRP sheet bonded to concrete. Construction and Building Materials 2015;82:206–218.
[20] Shi, J.W., Zhu, H., Wu, Z., Wu, G.. Experimental study of the strain rate effect of FRP sheet-concrete interface. Tumu Gongcheng Xuebao/China Civil Engineering Journal 2012;45:99–107.
[21] Shen, D., Shi, X., Ji, Y., Yin, F.. Strain rate effect on bond stress–slip relationship between basalt fiber-reinforced polymer sheet and concrete. Journal of Reinforced Plastics and Composites 2015;34(7):547–563.
[22] Bilotta, A., Di Ludovico, M., Nigro, E.. Frp-to-concrete interface debonding: Experimental calibration of a capacity model. Composites Part B: Engineering 2011;42(6):1539–1553.
[23] Aydin, H., Gravina, R.J., Visintin, P.. A partial-interaction approach for extracting FRP-to-concrete bond characteristics from environmentally loaded flexural tests. Composites Part B: Engineering 2018;132:214–228.
[24] Duvant, G., Lions, J.L.. Inequalities in mechanics and physics; vol. 219. Springer Science & Business Media; 2012.
[25] Wang, C., Liu, Z., Xia, B., Duan, S., Nie, X., Zhuang, Z.. Development of a new constitutive model considering the shearing effect for anisotropic progressive damage in fiber-reinforced composites. Composites Part B: Engineering 2015;75:288–297.
[26] Li, B., Li, Y., Su, J.. A combined interface element to simulate interfacial fracture of laminated shell structures. Composites Part B: Engineering 2014;58:217–227.
[27] Zhou, Y., Lu, Z., Yang, Z.. Progressive damage analysis and strength prediction of 2d plain weave composites. Composites Part B: Engineering 2013;47:220–229.
[28] Simo, J., Hughes, T.. Computational inelasticity. Springer-Verlag, New York 1998;.
[29] Carosio, A., Willam, K., Etse, G.. On the consistency of viscoplastic formulations. International Journal of Solids and Structures 2000;37(48):7349 – 7369. doi:\bibinfo{doi}{https://doi.org/10.1016/S0020-7683(00)00202-X}. URL http://www.sciencedirect.com/science/article/pii/S002076830000202X.
[30] JSCE-E-543-2000, test method for bond properties of continuous fiber sheets to concrete. Japan Society of Civil Engineers (JSCE), Tokyo, Japan: Research Committee on Upgrading of Concrete Structures with Use of Continuous Fiber Sheets 2001;.
[31] Sneed, L., D'Antino, T., Carloni, C., Pellegrino, C.. A comparison of the bond behavior of pbo-frcm composites determined by double-lap and single-lap shear tests. Cement and Concrete Composites 2015;64:37–48.